THE JOURNAL OF PHYSICAL CHEMISTRY LETTERS
A JOURNAL OF THE AMERICAN CHEMICAL SOCIETY

pubs.acs.org/JPCL
Letter

Correlating Rashba Suppression with Exciton Binding in Low-Dimensional Metal Halide Perovskites

Marco Antonio de Andrade Queiroz,* Danilo Neves Silveira, Fernando P. Sabino, Carlos M. O. Bastos, Celso R. C. Rêgo, Maurício J. Piotrowski, Alexandre C. Dias, and Diego Guedes-Sobrinho*

Cite This: https://doi.org/10.1021/acs.jpclett.6c01964

ABSTRACT: We used DFT-1/2+SOC band structures mapped to Wannier tight-binding Hamiltonians and solved with the Bethe−Salpeter equation to examine how confinement, polymorphism, and metal off-centering tune excitons in Pb- and Sn-iodide perovskites in 3D ($MA(Pb\ or\ Sn)I_3$), quasi-2D ($BA_2(PborSn)I_4$), and model quasi-1D ($BA_3(PborSn)I_5$). The 3D polymorphs show a clear trend: as symmetry increases from orthorhombic to tetragonal to pseudocubic, E_b decreases. At fixed dimensionality, restoring local metal-centered symmetry suppresses Rashba splitting. It reduces or preserves E_b, indicating that SOC affects excitons mainly through band-edge structure rather than direct strengthening of the electron−hole Coulomb kernel. Low-dimensional compounds retain much larger E_b than 3D analogs, although quasi-1D is not monotonic with quasi-2D. Photoluminescence spectra place the lowest excitons at the optical gap, consistent with bright ground-state excitons.

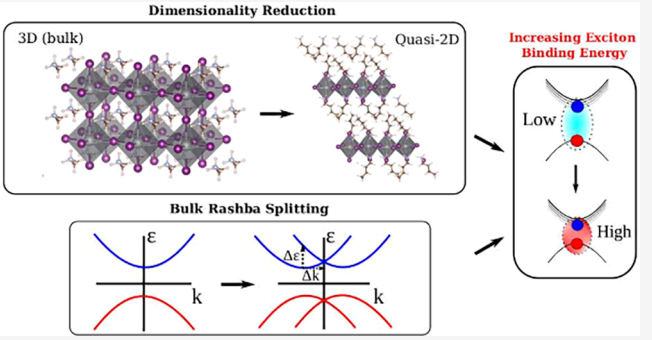

Metal-Halide Perovskites (MHPs) have been identified as promising semiconductors for solar cell applications and other optoelectronic devices, owing to advantages such as a wide compositional range and the ability to form 2D or 3D structures.[1−3] The atomistic profile becomes quite relevant regarding optoelectronic properties, such as band gaps and optical absorption, as atomic and electronic structures are correlated.[4,5] Dimensionality reduction in dielectric materials (from 3D → 2D → 1D) increases confinement effects, intensifying the interaction of electron−hole (*e-h*) pairs and leading to an enhanced exciton formation.[6,7] However, available data about these effects, along with the correlations between atomic arrangements and electronic structure, still remain scarce.

3D structures such as $MAPbI_3$ (MA^+ = methylammonium) are arranged by phase, following the orthorhombic → tetragonal → cubic transition as temperature increases.[8,9] Once the MA^+ cations are replaced by organic spacer cations (BA^+ = butylammonium), the structure assumes a quantum-well-like topology as a quasi-2D system.[10] This affects the physical properties, as low-dimensional systems are known for improved stability and larger band gaps.[11,12] Hybrid systems such as $BA_2MA_{n-1}Pb_nI_{3n+1}$ as n stacked layers provide a clear illustration on how the dimensionality reduction affects electronic properties, as for $n = \infty$ (bulk) the band gap shows a tendency to reach 1.55−1.67 eV, although for $n = 1$ (quasi-2D) the band gap is increased to 2.43 eV.[12] Moreover, these correlations still require further investigation once excitonic effects are included.

Lead-based MHPs exhibit strong spin−orbit coupling (SOC) effects, which are associated with local distortions such as metal-off centering within the octahedra, i.e., an induced breaking of inversion symmetry, leading to the bulk Rashba effect.[13−15] This phenomenon causes spin degeneracy breaking at the band edges, splitting them and consequently altering properties such as band gaps (direct → indirect) and charge-carrier lifetimes.[16,17] Currently, its impact on the excitonic properties is still unexplored. The exciton binding energies (E_b) have been measured for several MHPs. While $MAPbI_3$ displays low E_b values, ranging from 7 to 130 meV, the monolayered quasi-2D systems BA_2PbI_4 and BA_2SnI_4 (i.e., for $n = 1$) show 370 and 270 meV, respectively, indicating how structure and composition alter excitonic properties.[18,19] However, the bulk Rashba effect's specific role in systematically influencing the exciton binding energies considering MHPs throughout different dimensionalities requires more investigation.

A recent study on how Rashba physics influences nonradiative recombination in the quasi-2D system $3BrMBA_2PbI_4$ found a 20% increase in carrier lifetime associated with the Rashba

Received: June 14, 2026
Revised: July 14, 2026
Accepted: July 24, 2026

splitting.[20] While their work did not directly consider excitons, their findings suggest that Rashba-active distortions can impact optical and recombination processes. In this study, we address this issue by calculating excitonic properties for Pb- and Sn-based iodide perovskites in three confinement regimes: 3D $MAMI_3$, quasi-2D BA_2MI_4, and model quasi-1D BA_3MI_5, where M is either Pb^{2+} or Sn^{2+}. We use the quasi-1D structures as hypothetical models for confinement, not as predicted stable phases. We aim to clarify how dimensionality, polymorphism, and local metal off-centering influence Rashba splitting and exciton binding.

Below, we summarize our methodological approach through the workflow represented in Figure 1 (b).

i) First, DFT was employed for the electronic description through the semilocal exchange−correlation functional (based on the Perdew−Burke−Ernzerhof proposal, i.e., PBE) combined with spin−orbit coupling (SOC), in which empirical van der Waals (vdW) based on the Grimme-D3 correction was used.[21−25] For the total energy and structural optimization, we used the projector-augmented plane wave (PAW) by considering the explicit configurations of the valence electrons, e.g., H ($1s^1$), C ($2s^2$, $2p^2$), N ($2s^2$, $2p^3$), I ($5s^2$, $5p^5$), Pb ($5s^2$, $5d^{10}$, $6s^2$, $6p^2$), and Sn ($4d^{10}$, $5s^2$, $5p^2$), within the Vienna *Ab initio* Simulation Package (VASP) code,[26−28] in which fully relativistic calculations describe the core states. The plane waves were expanded up to a cutoff energy of 480 eV and the Brillouin zone integration was performed considering a *k*-mesh Γ-centered grid of **k** points for 3D structures of 8 × 8 × 8 for pseudocubic, 6 × 6 × 4 for tetragonal, and 6 × 4 × 5 for orthorhombic. For quasi-2D, 6 × 4 × 4 was employed, whereas 6 × 2 × 2 was used for quasi-1D. Finally, the Hellmann−Feynman forces were relaxed until their values were less than 0.010 eV $Å^{-1}$ in each atom.

ii) Moving for the band gap calculations, alternatively to the hybrid functionals and GW approximation (given their high computational cost associated),[2] we have applied the widely used DFT-1/2+SOC as a low cost approach.[4−6,12,29,30] Based on the Slater transition technique, the valence band is half-occupied by the 5p states of I, and the conduction band is dominated by the 6p states of Pb or the 5p states of Sn. Here, a modified Kohn−Sham potential is built up via $V_{mod,KS} = V_{KS}(\vec{r}) - V_s(\vec{r})$, where $V_{KS}(\vec{r})$ represents the standard Kohn−Sham potential and $V_s(\vec{r})$ is the self-energy potential, which is calculated through $V_s(\vec{r}) = \Theta(\vec{r}, CUT)[V_{ae}(\vec{r}) - V_{ae-1/2}(\vec{r})]$ from the optimized CUT parameter which maximize the band gap value (Figure S1 contains all CUT optimizations).

iii) Through the maximally localized Wannier functions we have built up the Hamiltonians—from the Wannier90 code[31]—for all the systems by aiming to access the excitonic properties through a tight-binding (TB) approach, in which the Bethe−Salpeter Equation (BSE)[32] is solved and the ground state of the exciton is obtained from a low computational effort in detriment to the *ab initio* approaches.

iv) Finally, TB-BSE solutions were obtained through the WanTiBEXOS code by taking a 3D Coulomb potential for the *e-h* pairwise interaction,[33] from which the ground state of the exciton (i.e., its optical band gap, E_{opt}), exciton band structure, and the optical absorption coefficient were calculated. Thus, the exciton binding energies were calculated through the difference between the fundamental and optical band gap, i.e., $E_b = E_g - E_{opt}$. Furthermore, the linear optical response was calculated within both the independent-particle approximation (IPA) and BSE to capture excitonic quasi-particle effects, as well as the photoluminescence peaks at 300 K.[34] Details regarding possible configurations and other code definitions are presented in the Supporting Information (Table S1). Although the systems are referred to as quasi-2D and quasi-1D based on the connectivity of the inorganic framework, the octahedral layers/wires are separated only by the organic spacer cations, without vacuum interfaces. Therefore, the simulations employ fully periodic three-

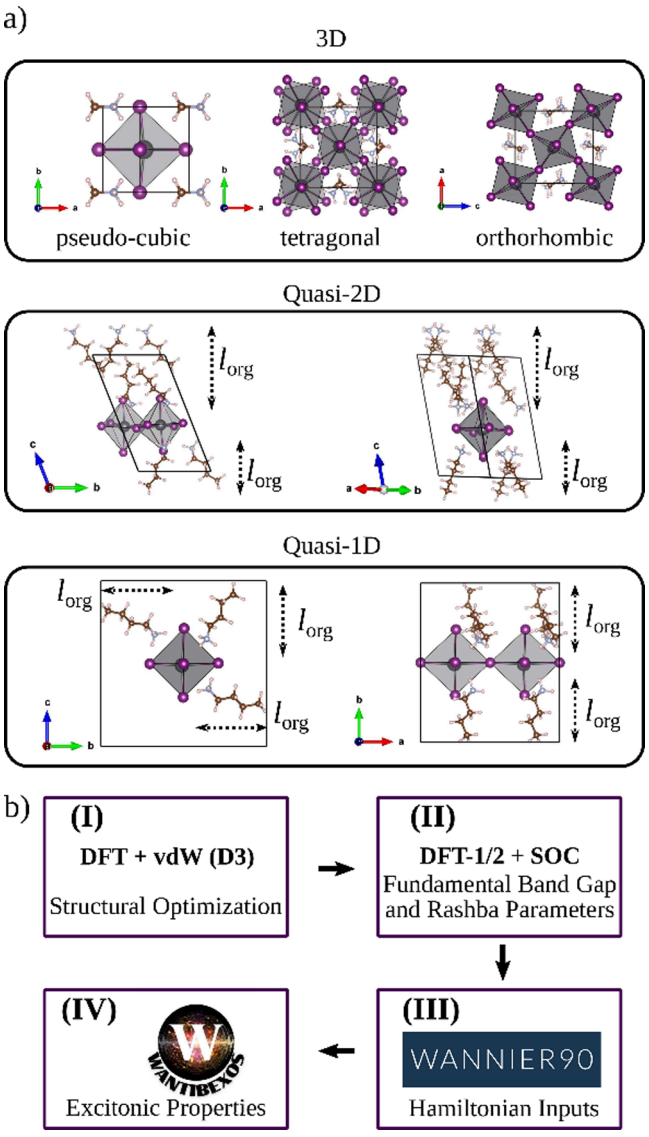

Figure 1. a) Unit cell representation of the investigated structures, from 3D (pseudocubic, tetragonal, and orthorhombic phases) to quasi-2D and quasi-1D (l_{org} depicts the length of the organic layer through the BA^+ spacer cation). b) Methodology workflow: (I) geometry optimization done through DFT with the addition of vdW correction; (II) electronic structure characterization (including the fundamental band gap and Rashba parameters determination) done with DFT through the employment of DFT-1/2 correction and addition of SOC effects; (III) Wannierization step to generate the Hamiltonian inputs; (IV) TB-BSE, done through WanTiBEXOS, to calculate the excitonic properties.

https://doi.org/10.1021/acs.jpclett.6c01964
J. Phys. Chem. Lett. XXXX, XXX, XXX−XXX

dimensional crystal structures, in which a 3D Coulomb interaction was used throughout the calculations.

In a comparative analysis of our structural data with experiments (as detailed in Table S2 in the Supporting Information),[11,35−37] we have obtained small deviations for the lattice parameters through the optimization process of the 3D and quasi-2D, which indicates that the DFT+D3 protocol is suitable for the different dimensionalities. For instance, for *a*, *b*, and *c* parameters in $MAPbI_3$ ($MASnI_3$) as pseudocubic, tetragonal, and orthorhombic, the deviations did not overcome 2.5% (2.8%). For quasi-2D monolayered BA_2PbI_4 (BA_2SnI_4) systems, the deviations were less than −1.0% (−1.2%). Furthermore, the larger deviation observed along the organic stacking direction, as depicted in Figure 1(a) as l_{org}, is consistent with previous DFT studies and reflects the strong temperature dependence of the organic spacer arrangement.[12,19,38] Conversely, for quasi-1D structures, it is important to note that they should be regarded as hypothetical model systems intended to investigate confinement trends, not as predicted stable phases; therefore, there are no experimental data for comparative analysis.

On the other hand, for all the dimensionalities, the metal off-centering magnitude (as a symmetry-breaking pattern associated with the bulk Rashba effect over strong metal spin−orbit coupling) is characterized by the local octahedral distortions from M−I bond lengths. These bonds split in short−large lengths, given the MA^+ cations in the 3D systems employ different distortion patterns into the pseudocubic, tetragonal, and orthorhombic structures. While this M−I bond splitting is pronounced for pseudocubic and tetragonal structures, this feature vanishes entirely for the orthorhombic structures, given the alignment of the tilting between different octahedral layers, yielding simultaneously nearly centrosymmetric octahedra and equally aligned MA^+ cations with canceled dipole moments. With platonic-like octahedra (as shown in Table S2), the orthorhombic phase does not present bond-length asymmetries responsible for local inversion-symmetry breaking.

To distinguish the effects of local inversion-symmetry breaking from those of dimensional confinement, we made two structural variants for each composition and dimensionality. The fully relaxed structures are called metal-off because they retain the local M−I bond-length asymmetry and octahedral distortions associated with the local distortion known as the metal off-centering process. We created the metal-on structures by moving the metal atom to the center of the octahedron (metal on-centering process), removing the short and long M−I bond difference, and setting the relevant M−I−M angles to 180°, while keeping the relaxed unit-cell volume the same. These metal-on structures serve as idealized high-local-symmetry references, not as new thermodynamic phases. This approach lets us test how restoring local symmetry affects Rashba splitting and exciton binding at fixed composition and dimensionality. The octahedral-tilt patterns are shown using Glazer notation in Figure S2 in the Supporting Information.[44]

The values of electronic band gap energies (E_g) for both Pb and Sn systems as 3D systems in pseudocubic and tetragonal, monolayered quasi-2D (i.e., $n = 1$), and model quasi-1D fully relaxed are summarized in Figure 2. Our DFT-1/2+SOC protocol provided a set of E_g values in excellent agreement with experiments ($E_{g,exp}$). For instance, $MAPbI_3$ as pseudocubic (tetragonal) reaches 1.52 eV (1.54 eV), deviating in 2.7% (1.3%) given the 1.48 eV[40] (1.52 eV)[39] experimentally reported.

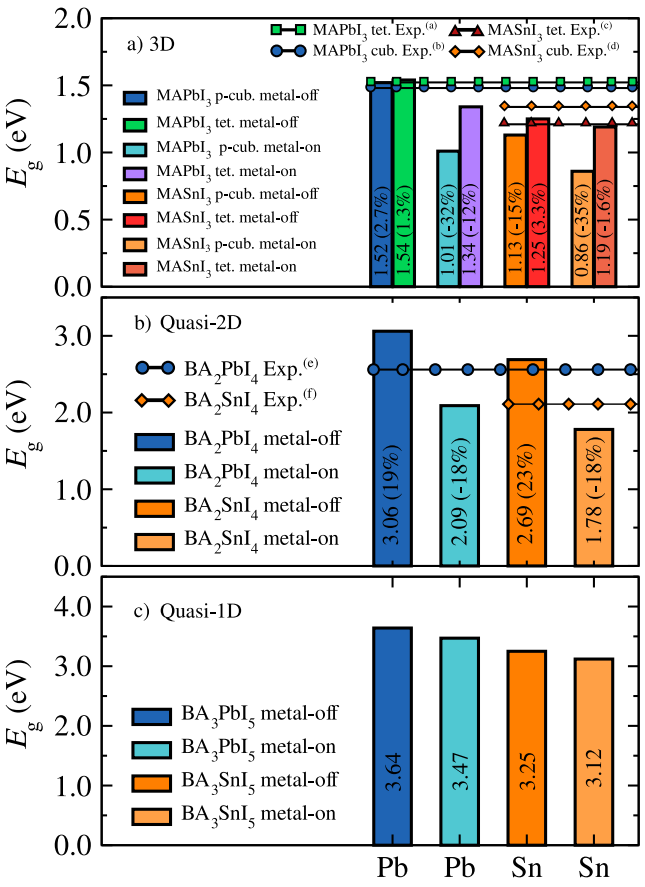

Figure 2. Electronic band gap energies based on DFT-1/2+SOC protocol for the a) 3D $MAPbI_3$ and $MASnI_3$ structures as metal-off in pseudocubic and tetragonal phases, b) quasi-2D BA_2PbI_4 and BA_2SnI_4, and c) quasi-1D BA_3PbI_5 and BA_3SnI_5, all the configurations with their metal-on counterparts. The horizontal lines refer to experimental values for $MAPbI_3$ in tetragonal phase (green squares, 1.52 eV),[39] $MAPbI_3$ in pseudocubic phase (blue circles, 1.48 eV),[40] $MASnI_3$ in tetragonal phase (red triangles, 1.21 eV),[11] $MASnI_3$ in pseudocubic phase (orange diamonds, 1.33 eV),[41] BA_2PbI_4 (2.56 eV),[42] and BA_2SnI_4 (2.18 eV).[43]

Similarly to $MASnI_3$ as pseudocubic (tetragonal), E_g = 1.13 eV (1.25 eV) value deviates only −15% (3.3%) from the 1.33 eV[1] (1.21 eV),[11] so that this behavior is kept for the orthorhombic $MAPbI_3$ with deviation not higher than −5.9% (as shown in Table S3 in the Supporting Information, which contains all the obtained E_g and experimental references when available).

For 3D → quasi-2D changing as an enhancement of the confinement effects, BA_2PbI_4 (BA_2SnI_4) reaches a fundamental band gap of E_g = 3.06 eV (2.69 eV). These values are higher by 19% (23%) than the optical band gap of E_{opt} = 2.56 eV (2.18 eV) from experiments based on temperature-dependent photoluminescence and transient absorption (TA) spectroscopy (electroabsorption (EA) spectroscopy) techniques in which the excitonic effects are captured (so that E_{opt} concerns the exciton ground state). The values for the hypothetical quasi-1D systems BA_3PbI_5 and BA_3SnI_5 are E_g = 3.64 and 3.25 eV, respectively, showing the increase of the confinement effect associated with the enhancement of the opening band gap. These results provide a quantitative picture of the dimensionality reduction correlated with the fundamental band gap broadening, given the reduction of electronic states on the band edge.

https://doi.org/10.1021/acs.jpclett.6c01964
J. Phys. Chem. Lett. XXXX, XXX, XXX−XXX

One observes in Figure 2 a decrease in the band gap—i.e, E_g(off) > E_g(on)—for the Pb and Sn systems in all dimensionalities. The metal off-centering → on-centering changes yield a higher *sp* hybridization that forms the valence top (which also lies closer to the vacuum) when equatorial and apical M−I−M angles are 180° for the platonic-like configurations (i.e., metal on-centering and no octahedral tilting). For instance, the $a^0a^0a^0$ platonic centrosymmetric as 3D pseudocubic (tetragonal) configuration yields gap energies of 1.01 eV (1.34 eV) for the $MAPbI_3$, whereas for $MASnI_3$ the E_g was reduced to 0.86 eV (1.19 eV).

For the quasi-2D systems this behavior is more pronounced given the reduced BA_2PbI_4 (BA_2SnI_4) E_g(off → on) values of 3.06 eV → 2.09 eV (2.69 eV → 1.78 eV). We observed that quasi-2D MHPs are more sensitive to local distortions and octahedral geometry than their bulk counterparts, exhibiting a band gap closure of around 1 eV upon the metal-off → metal-on transition, compared to only about 0.3 eV in the bulk. This behavior can be comprehensively justified by the presence of relative octahedral tilting in the quasi-2D metal-off structures, which is completely absent in the metal-on structures. Hence, the gap reduction results from a combination of both metal-on-centering and the suppression of relative octahedral tilting. In all remaining investigated systems, the reduction via the metal-off → metal-on transition is primarily due to the metal on-centering process and is therefore less drastic. For instance, in the conceived quasi-1D structures, the effect of the off → on transition on band gap narrowing is more modest, with E_g values changing from 3.64 to 3.47 eV for BA_3PbI_5 and from 3.25 to 3.12 eV for BA_3SnI_5.

From the band structures calculated through the DFT-1/2+SOC protocol (Figures S3 and S4) we have quantified the Rashba splitting effect along some paths in the Brillouin zone. The M ← R (X ← Γ) and R → Γ (Γ → Z) branches were employed for pseudocubic (tetragonal) as 3D structures, as well as X ← Γ and Γ → M for quasi-2D. For quasi-1D, we have considered only the periodic direction for the octahedral connections along X ← Γ. Figure 3 depicts the Rashba parameters ($\alpha = \Delta\varepsilon/2\Delta k$) calculated through the ε wells vertices correlated with a particular *k*-points ($\Delta k = |k - k_0|$) for the valence (ε_V) and conduction (ε_C) bands; numerical details are available in Table S4 in Supporting Information.[13,45]

For all dimensionalities, one observes $\alpha_C \geq \alpha_V$, given the higher contributions of the metal-*p* orbital for the conduction band maximum associated with their SOC. For instance, for $MAPbI_3$ pseudocubic (tetragonal) we found the highest $\alpha_C \sim$ 1.52 eVÅ (~0.46 eV Å) for the M ← R (X ← Γ) branch, where for $MASnI_3$ $\alpha_C \sim$ 0.99 eVÅ (~0.49 eV Å) is the highest value, from which the tendencies based on $\alpha_{p\text{-cub.}} > \alpha_{tet.}$ are in agreement with previous bulk Rashba characterizations.[15] Therefore, while one observes a suppression of pseudocubic → tetragonal changing due to the fitting of the MA^+ cations into the cavities resulting from the out-of-phase rotation of the octahedra, which shortens the bond length deviations and approximates the metal to the octahedron center, for orthorhombic structures α is fully suppressed since the MA^+ cations fit optimally for the in-phase octahedral rotations. As a result, the presenting bond-length asymmetries responsible for local inversion-symmetry breaking are eliminated, consequently suppressing the bulk Rashba splitting ($\alpha_{v,c} \sim 0$ eV Å).

Quasi-2D and model quasi-1D systems usually show the same pattern, where α_C is equal to or greater than α_V. The only exception is BA_3SnI_5, where α_C is a bit smaller than α_V. This

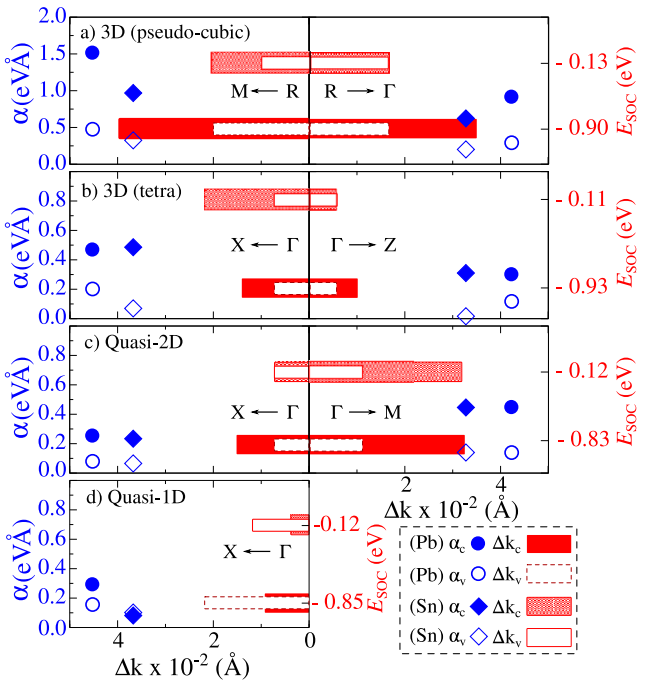

Figure 3. Rashba splitting parameters (blue) with respect to the Δk, including SOC energies (red) calculated for the metal-off systems. The blue-filled circle and nonfilled circle show, respectively, the α_c and α_v values for the Pb-based systems, while the blue-filled and nonfilled diamonds show, respectively, the α_c and α_v values for the Sn-based systems. The red bars, each one with a different fill or line pattern, represent the Δk_c and Δk_v values, aligned with the SOC energies for Sn and Pb. Panels a), b), c), and d) refer, respectively, to 3D systems as pseudocubic, tetragonal, quasi-2D systems, and quasi-1D systems.

happens because the quasi-1D structure has incomplete iodine coordination, which increases the iodine's role at the top of the valence band. Compared to 3D structures, these lower-dimensional systems have smaller Rashba parameters. This arises from two distinct mechanisms. First, the BA^+ spacer cations in the quasi-2D (and quasi-1D) systems exhibit characteristics that contrast with the 3D composition: with the NH_3^+ dipole moment oriented toward the layers, its dipole moment effect is mitigated, unlike in 3D systems, where dipole moments are aligned along a single direction. Second, the greater degrees of freedom within the octahedral network may favor the centering of the metal atom within the octahedron. Together, these two effects result in reduced distortion of the octahedral network and a smaller displacement of the metal atom from the center.

Still, the SOC contributions are significant: E_{SOC}, the accumulated energy contribution arising from SOC, ranges from approximately −0.93 to −0.83 eV for Pb-based systems and from approximately −0.13 to −0.11 eV for Sn-based systems. The horizontal spin splitting, measured by Δk_V and Δk_C, reflects local inversion-symmetry breaking more than just SOC strength. Overall, $\Delta k_{C,V}$(Pb) is greater than $\Delta k_{C,V}$(Sn), which matches the fact that Pb has stronger SOC. This also leads to another general trend, since the magnitude of the bulk Rashba effect is primarily determined by local distortions and SOC energies. At fixed symmetry, one observes that $\alpha_{v,c(Pb)} \geq \alpha_{v,c(Sn)}$, demonstrating how Rashba can be modulated according to composition.

Next, we evaluate the excitonic properties using the TB-BSE solution with Wannier Hamiltonians fitted to the DFT-1/

https://doi.org/10.1021/acs.jpclett.6c01964
J. Phys. Chem. Lett. XXXX, XXX, XXX−XXX

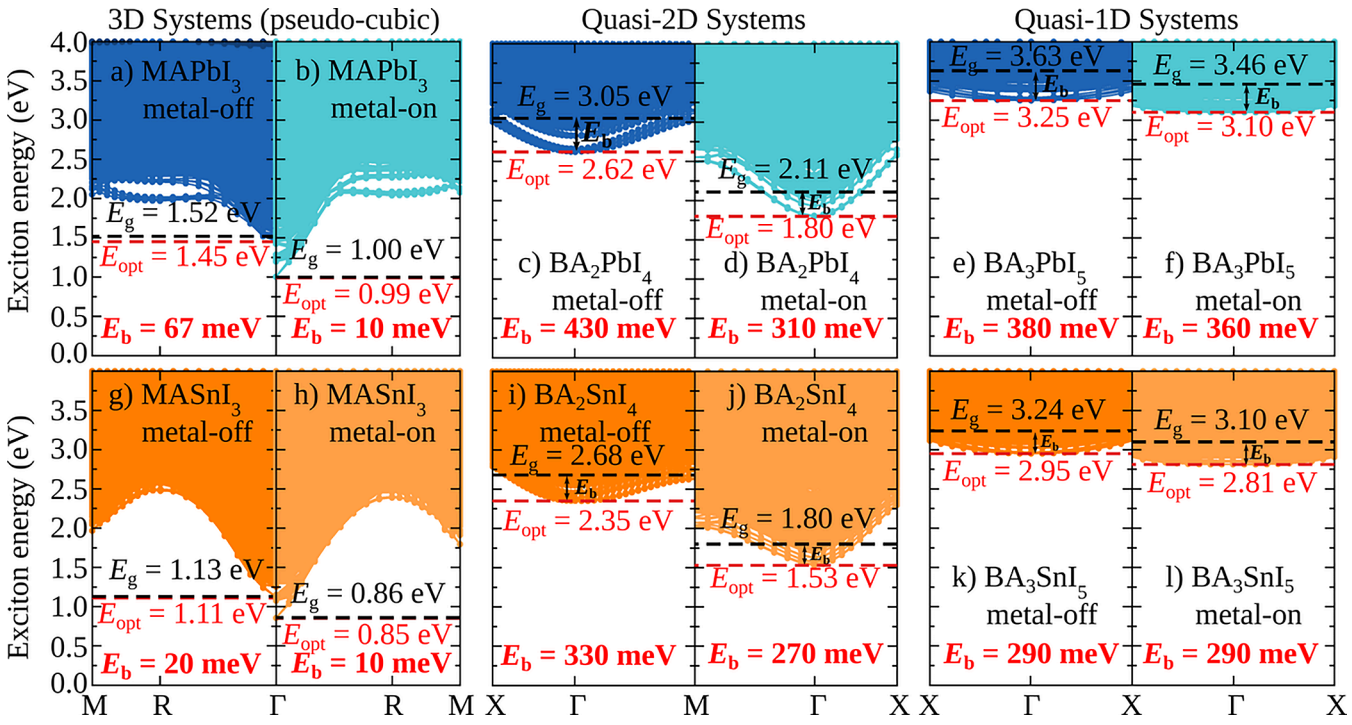

Figure 4. Calculated exciton band structures and exciton binding energies (E_b) for representative systems of our investigation. The blue and cyan panels refer to the Pb-based systems, while the orange and light orange panels represent the Sn-based systems. The panels refer to a) 3D $MAPbI_3$ metal-off, b) 3D $MAPbI_3$ metal-on, c) quasi-2D BA_2PbI_4 metal-off, d) quasi-2D BA_2PbI_4 metal-on, e) quasi-1D BA_3PbI_5 metal-off, f) quasi-1D BA_3PbI_5 metal-on, g) 3D $MASnI_3$ metal-off, h) 3D $MASnI_3$ metal-on, (i) quasi-2D BA_2SnI_4 metal-off, j) quasi-2D BA_2SnI_4 metal-on, k) quasi-1D BA_3SnI_5 metal-off, l) quasi-1D BA_3SnI_5 metal-on.

2+SOC band structures (Figures S3 and S4 in the Supporting Information). Figure 4 presents typical exciton band structures. In the 3D systems, the exciton ground states are found at the high-symmetry point Γ in the pseudocubic, and also in tetragonal and orthorhombic structures, as shown in Figure S5. This result indicates that the lowest-energy excitons are bright.

Dimensional confinement leads to the largest increase in exciton binding as a dominant effect for the correlation between structure and E_b magnitude. For instance, in quasi-2D systems, E_b = 430 meV for BA_2PbI_4 and 330 meV for BA_2SnI_4, both much higher than the 3D as pseudocubic, tetragonal, and orthorhombic E_b values. On the other hand, the metal-off → metal-on transformation yields an increment on the E_b decreasing as a secondary effect, since these values drop to 310 and 270 meV Pb- and Sn-based quasi-2D systems. This effect is also observed for the 3D phases throughout the crystallographic symmetry increasing from orthorhombic to tetragonal to pseudocubic, i.e., E_b decreases. For $MAPbI_3$, E_b drops from 240 meV in the orthorhombic phase to 220 meV in the tetragonal phase, and then to 67 meV in the pseudocubic phase, whereas for $MASnI_3$, the values follow a similar trend: 190, 160, and 20 meV. Advancing for the metal-off → metal-on transition, since for orthorhombic systems the metal-off and -on structures are equivalent and E_b does not change, for tetragonal $MAPbI_3$ ($MASnI_3$), E_b reduces to 180 meV (150 meV), whereas for pseudocubic reduces to 10 meV (10 meV).

The Rashba suppression modifies the band edges, which are associated with the spin nature of the charge carriers. With significant Rashba splitting, the valence band maximum (VBM) and conduction band minimum (CBM) display opposite spin textures, resulting in a (slower) spin-forbidden radiative recombination transition. Once the Rashba effect is weakened, VBM and CBM now exhibit aligned spin textures, leading to a (faster) spin-allowed recombination dynamics. Our results complement this mechanism, now associating the switch from spin-forbidden to spin-allowed transitions with a decrease in exciton binding energies. Moreover, it is important to mention that the observed reduction in exciton binding energy accompanying Rashba suppression should be interpreted as part of a broader modification of the electronic structure rather than as evidence of a direct causal relationship, since effective masses, band-edge dispersion, orbital localization, and dielectric screening are all expected to evolve simultaneously. Consequently, the present calculations do not allow these individual contributions to be quantitatively disentangled. For instance, the theoretical quasi-1D systems also have stronger binding than their 3D counterparts, with E_b = 380 meV for BA_3PbI_5 and 290 meV for BA_3SnI_5. However, E_b does not continue to increase from quasi-2D to quasi-1D, given the last ones are slightly lower by showing that confinement is not the only factor affecting binding energy.

The lower E_b values in Sn-based systems compared to Pb-based ones match their different SOC strengths and band-edge characters, but this difference should not be seen as a direct Coulomb effect of SOC alone. Table S5 in the Supporting Information presents the calculated electron and hole effective masses. The reduced effective masses follow the same qualitative trends observed for the exciton binding energies, including the decrease from metal-off to metal-on configurations and the larger values found in low-dimensional systems. However, the effective masses alone do not fully account for the observed variations in the E_b. In particular, the quasi-2D and model quasi-1D systems exhibit similar reduced masses while displaying

https://doi.org/10.1021/acs.jpclett.6c01964
J. Phys. Chem. Lett. XXXX, XXX, XXX−XXX

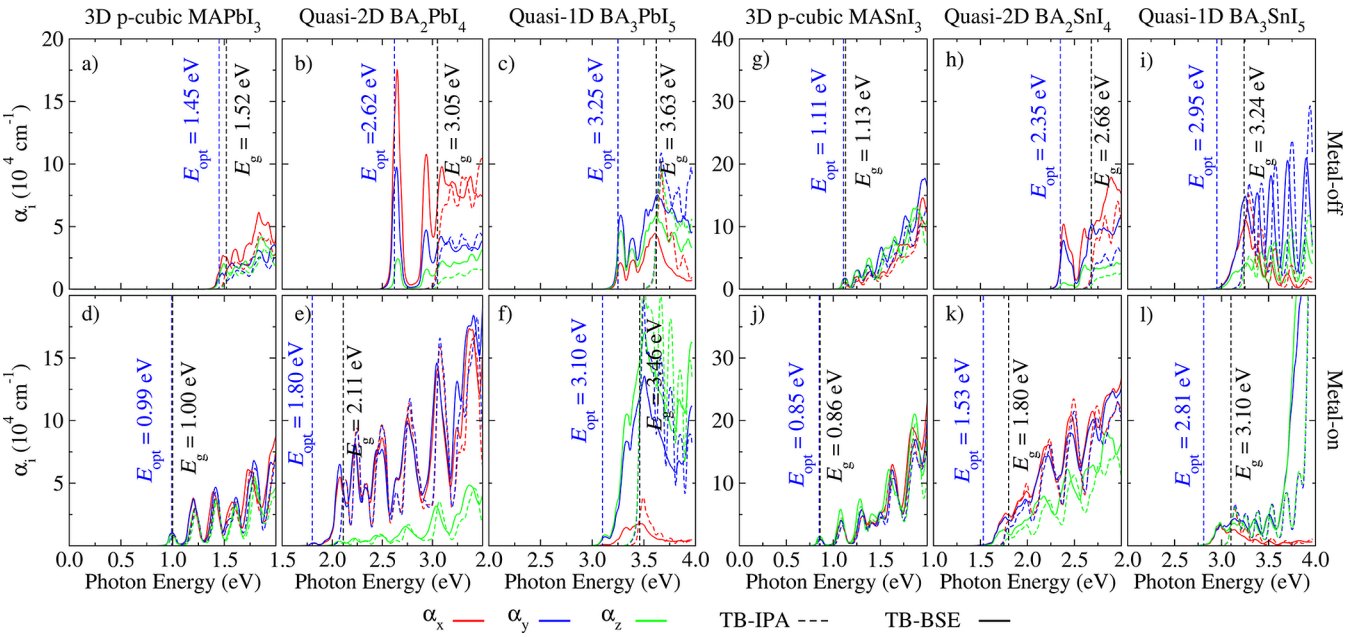

Figure 5. Absorption coefficient (α) calculated through independent particle approximation ((W)TB+IPA as dashed lines) and through (W)TB+BSE formalism (solid lines) for the excitonic effects. The red, blue, and green colors represent α along the *x*-, *y*-, and z-axes. The values of electronic band gap (E_g) and optical band gap (E_{opt}) are depicted in each graphic. The first-row panels depict metal-off structures, while the second-row panels depict metal-on structures. The panels refer to a) 3D $MAPbI_3$ metal-off, b) quasi-2D BA_2PbI_4 metal-off, c) quasi-1D BA_3PbI_5 metal-off, d) 3D $MAPbI_3$ metal-on, e) quasi-2D BA_2PbI_4 metal-on, f) quasi-1D BA_3PbI_5 metal-on, g) 3D $MASnI_3$ metal-off, h) quasi-2D BA_2SnI_4 metal-off, (i) quasi-1D BA_3SnI_5 metal-off, j) 3D $MASnI_3$ metal-on, k) quasi-2D BA_2SnI_4 metal-on, l) quasi-1D BA_3SnI_5 metal-on.

different exciton binding energies, indicating that dielectric screening, orbital localization, and band edge dispersion also contribute significantly. Therefore, the effective mass analysis supports the observed qualitative trends but does not uniquely determine the exciton binding energies.

We further analyzed the linear optical response through the absorption coefficients for $\hat{x}$, $\hat{y}$, and $\hat{z}$ polarizations (Figure 5 and Figure S6 in the Supporting Information). The spectra were evaluated from 0.0 to 2.0 eV for the 3D systems and from 0.0 to 4.0 eV for the quasi-2D and quasi-1D systems. Comparing IPA and BSE spectra shows that excitonic effects red shift the optical onset in all dimensionalities. For pseudocubic $MAPbI_3$ and $MASnI_3$, the metal-off → metal-on transformation makes the optical response more isotropic and strongly reduces the separation between E_g and E_{opt}. This behavior follows from the restoration of local metal-centered symmetry and the associated modification of band-edge hybridization.

In quasi-2D BA_2PbI_4 and BA_2SnI_4, the in-plane components α_x and α_y are the main contributors to absorption near the optical onset. The out-of-plane response α_z depends strongly on the direction of the organic spacer. Figure S7 in the Supporting Information shows the project density of states (PDOS) for our low-dimensionality systems. For the hypothetical quasi-1D systems BA_3PbI_5 and BA_3SnI_5, the optical response is highly anisotropic and stays that way after the metal-off to metal-on transformation, which matches the wire-like structure of the inorganic framework. One way to explain this α_i anisotropy in quasi-1D systems is to analyze the contributions of iodine atoms along the wire axis versus those extending beyond the wire periodicity, using the PDOS for localized iodine atoms, as shown in Figure S8 in the Supporting Information. Interestingly, the iodine atoms located outside the periodicity of the wire are found to contribute much more significantly to the electronic states at the valence band-edge, which explains why α_z and α_y dominates so strongly over the in-plane components in these systems. The calculated photoluminescence spectra at 300 K (Figures S9 and S10 in the Supporting Information) have emission peaks that match E_{opt}, which confirms that the lowest emissive excitons are bright.

Our results show that dimensionality, polymorphism, and local metal off-centering influence excitonic effects in Pb- and Sn-based iodide metal halide perovskites. We used DFT-1/2+SOC band structures, mapped onto Wannier tight-binding Hamiltonians, and solved the resulting Hamiltonians using the Bethe−Salpeter equation. In 3D polymorphs, we found a clear trend: the exciton binding energy (E_b) decreases from orthorhombic to tetragonal to pseudocubic structures. When composition and dimensionality are fixed, changing from metal-off to metal-on restores local metal-centered symmetry, reduces Rashba splitting, and generally lowers the exciton binding energy. Our findings demonstrate that dimensional confinement remains as the dominant factor governing exciton binding energies. Nevertheless, the metal-off → metal-on transition at fixed composition and dimensionality plays a secondary role by modifying the band-edge electronic structure. However, Rashba-active distortions should be interpreted as part of a broader electronic structure modification involving band-edge dispersion, effective masses, orbital character, and dielectric screening, all of which contribute to the observed excitonic behavior. Quasi-2D BA_2PbI_4/BA_2SnI_4 and theoretical quasi-1D BA_3PbI_5/BA_3SnI_5 have much larger E_b than their 3D counterparts. However, the quasi-1D values are not higher than the quasi-2D values, which means that confinement, orbital character, and band dispersion all play a role. Our calculated photoluminescence spectra also show that the lowest-emission excitons appear at E_{opt} across all the systems we studied.

https://doi.org/10.1021/acs.jpclett.6c01964
J. Phys. Chem. Lett. XXXX, XXX, XXX−XXX

■ ASSOCIATED CONTENT

Supporting Information

The Supporting Information is available free of charge at https://pubs.acs.org/doi/10.1021/acs.jpclett.6c01964.

Extra results for the geometric and electronic properties (PDF)

■ AUTHOR INFORMATION

Corresponding Authors

Marco Antonio de Andrade Queiroz − *Quantum Chemistry and Thermodynamic Materials Group, Department of Chemistry, Federal University of Paraná, CEP, 81531-980 Curitiba, Brazil;* orcid.org/0009-0006-7507-4794; Email: marco.queiroz@ufpr.br

Diego Guedes-Sobrinho − *Quantum Chemistry and Thermodynamic Materials Group, Department of Chemistry, Federal University of Paraná, CEP, 81531-980 Curitiba, Brazil;* orcid.org/0000-0002-3313-2822; Email: guedes.sobrinho.d@gmail.com

Authors

Danilo Neves Silveira − *Quantum Chemistry and Thermodynamic Materials Group, Department of Chemistry, Federal University of Paraná, CEP, 81531-980 Curitiba, Brazil;* orcid.org/0000-0001-6343-5560

Fernando P. Sabino − *Materials Engineering Department, Engineering School of São Carlos, University of São Paulo, CEP, 13566-590 São Carlos, Brazil*

Carlos M. O. Bastos − *Institute of Physics and International Center for Physics, University of Brasília, Brasília, DF 70919-970, Brazil; Computational Materials Laboratory, LCCMat, Institute of Physics, University of Brasília, 70910-900 Brasília, Brazil*

Celso R. C. Rêgo − *Institute of Nanotechnology Hermann-von-Helmholtz-Platz, Karlsruhe Institute of Technology, 76021 Karlsruhe, Germany;* orcid.org/0000-0003-1861-2438

Maurício J. Piotrowski − *Department of Physics, Federal University of Pelotas, Pelotas, RS 96010-900, Brazil;* orcid.org/0000-0003-3477-4437

Alexandre C. Dias − *Institute of Physics and International Center for Physics, University of Brasília, Brasília, DF 70919-970, Brazil; Computational Materials Laboratory, LCCMat, Institute of Physics, University of Brasília, 70910-900 Brasília, Brazil*

Complete contact information is available at: https://pubs.acs.org/10.1021/acs.jpclett.6c01964

Funding

The Article Processing Charge for the publication of this research was funded by the Coordenacao de Aperfeicoamento de Pessoal de Nivel Superior (CAPES), Brazil (ROR identifier: 00x0ma614).

Notes

The authors declare no competing financial interest.

■ ACKNOWLEDGMENTS

The authors thank the Ogun Computer at CIMATEC SENAI (Salvador − BA), "Centro Nacional de Processamento de Alto Desempenho em São Paulo" (CENAPAD-SP, UNICAMP/FINEP - MCTI, relative to the projects n.897 and n.570), Lobo Carneiro HPC (NACAD) at the Federal University of Rio de Janeiro (UFRJ, project n.133), and SDumont supercomputer for the support to perform the calculations. The authors gratefully acknowledge the Karlsruhe Institute of Technology (KIT) for the HoreKa supercomputer resources. M.A.A.Q. thanks the Coordination for Improvement of Higher Level Education − CAPES (finance Code 001) for funding. The authors are also thankful for financial support from the National Council for Scientific and Technological Development (CNPq, grant numbers 409792/2024-1, 307345/2021-1, 408144/2022-0, 313081/2017-4, 303206/2025-0, 444431/2024-1, and 305335/2020-0), Federal District Research Support Foundation (FAPDF, grants 00193-00001817/2023-43 and 00193-00002073/2023-84), the Coordination for Improvement of Higher Level Education (CAPES), the Rio Grande do Sul Research Foundation (FAPERGS, grant number 24/2551-0001551-5). The project (HGF ZT-I-PF-5-261 GENIUS) underlying this publication was funded by the Initiative and Networking Fund of the Helmholtz Association in the framework of the Helmholtz AI project call.

■ REFERENCES

(1) Hao, F.; Stoumpos, C. C.; Cao, D. H.; Chang, R. P. H.; Kanatzidis, M. G. Lead-Free Solid-State Organic-Inorganic Halide Perovskite Solar Cells. *Nat. Photonics* **2014**, *8*, 489−494.

(2) Umari, P.; Mosconi, E.; De Angelis, F. Relativistic GW calculations on $CH_3NH_3PbI_3$ and $CH_3NH_3SnI_3$ Perovskites for Solar Cell Applications. *Sci. Rep.* **2014**, *4*, 4467.

(3) Zhang, J.; Shang, M.-h.; Wang, P.; Huang, X.; Xu, J.; Hu, Z.; Zhu, Y.; Han, L. n-Type Doping and Energy States Tuning in $CH_3NH_3Pb_{1-x}Sb_{2x/3}I_3$ Perovskite Solar Cells. *ACS Energy Lett.* **2016**, *1*, 535−541.

(4) de Araujo, L. O.; Rêgo, C. R.; Wenzel, W.; Silveira, D. N.; Piotrowski, M. J.; Sabino, F. P.; Pramudya, Y.; Guedes-Sobrinho, D. How Cation Nature Controls the Bandgap and Bulk Rashba Splitting of Halide Perovskites. *J. Comput. Chem.* **2023**, *44*, 1395−1403.

(5) Octavio de Araujo, L.; Rego, C. R. C.; Wenzel, W.; Sabino, F. P.; Guedes-Sobrinho, D. Impact of the Polymorphism and Relativistic Effects on the Electronic Properties of Inorganic Metal Halide Perovskites. *J. Phys. Chem. C* **2022**, *126*, 2131−2140.

(6) Silveira, D. N.; Dias, A. C.; de Araujo, L. O.; Queiroz, M. A.; Dalmedico, J. F.; de Oliveira Bastos, C. M.; Rêgo, C. R.; Piotrowski, M. J.; Guedes-Sobrinho, D. Excitonic Properties and Solar Harvesting Performance of $Cs_2ZnY_2X_2$ as Quasi−2D Mixed−Halide Perovskites. *J. Alloys Compd.* **2024**, *1007*, 176434.

(7) Mauck, C. M.; Tisdale, W. A. Excitons in 2D organic−inorganic halide perovskites. *Trends Chem.* **2019**, *1*, 380−393.

(8) Alaei, A.; Circelli, A.; Yuan, Y.; Yang, Y.; Lee, S. S. Polymorphism in metal halide perovskites. *Mater. Adv.* **2021**, *2*, 47−63.

(9) Kim, T. W.; Uchida, S.; Matsushita, T.; Cojocaru, L.; Jono, R.; Kimura, K.; Matsubara, D.; Shirai, M.; Ito, K.; Matsumoto, H.; Kondo, T.; Segawa, H. Self-Organized Superlattice and Phase Coexistence inside Thin Film Organometal Halide Perovskite. *Adv. Mater.* **2018**, *30*, 1705230.

(10) Ning, W.; Gao, F. Structural and functional diversity in lead-free halide perovskite materials. *Adv. Mater.* **2019**, *31*, 1900326.

(11) Stoumpos, C. C.; Malliakas, C. D.; Kanatzidis, M. G. Semiconducting Tin and Lead Iodide Perovskites with Organic Cations: Phase Transitions, High Mobilities, and Near-Infrared Photoluminescent Properties. *Inorg. Chem.* **2013**, *52*, 9019−9038.

(12) Guedes-Sobrinho, D.; Neves Silveira, D.; de Araujo, L. O.; Favotto Dalmedico, J.; Wenzel, W.; Pramudya, Y.; Piotrowski, M. J.; Rêgo, C. R. Revealing the Impact of Organic Spacers and Cavity Cations on Quasi-2D Perovskites via Computational Simulations. *Sci. Rep.* **2023**, *13*, 4446.

(13) Mosconi, E.; Etienne, T.; De Angelis, F. Rashba Band Splitting in Organohalide Lead Perovskites: Bulk and Surface Effects. *J. Phys. Chem. Lett.* **2017**, *8*, 2247−2252.
(14) Isarov, M.; Tan, L. Z.; Bodnarchuk, M. I.; Kovalenko, M. V.; Rappe, A. M.; Lifshitz, E. Rashba Effect in a Single Colloidal $CsPbBr_3$ Perovskite Nanocrystal Detected by Magneto-Optical Measurements. *Nano Lett.* **2017**, *17*, 5020−5026.
(15) Octavio de Araujo, L.; Sabino, F. P.; Rego, C. R. C.; Guedes-Sobrinho, D. Bulk Rashba Effect Splitting and Suppression in Polymorphs of Metal Iodine Perovskites. *J. Phys. Chem. Lett.* **2021**, *12*, 7245−7251.
(16) Zheng, F.; Tan, L. Z.; Liu, S.; Rappe, A. M. Rashba Spin-Orbit Coupling Enhanced Carrier Lifetime in $CH_3NH_3PbI_3$. *Nano Lett.* **2015**, *15*, 7794−7800.
(17) Zheng, F.; Tan, L. Z.; Liu, S.; Rappe, A. M. Correction to Rashba Spin−Orbit Coupling Enhanced Carrier Lifetime in $CH_3NH_3PbI_3$. *Nano Lett.* **2016**, *16*, 7316−7316.
(18) Gélvez-Rueda, M. C.; Hutter, E. M.; Cao, D. H.; Renaud, N.; Stoumpos, C. C.; Hupp, J. T.; Savenije, T. J.; Kanatzidis, M. G.; Grozema, F. C. Interconversion between Free Charges and Bound Excitons in 2D Hybrid Lead Halide Perovskites. *J. Phys. Chem. C* **2017**, *121*, 26566−26574. PMID: 29218073
(19) Dalmedico, J.; Silveira, D.; Bastos, C. M. O.; C Rego, C.; Cavalheiro Dias, A.; Guedes-Sobrinho, D.; Piotrowski, M. J. BA_2SnI_4 as a Promising 2D Ruddlesden−Popper Perovskite for Optoelectronic Applications. *J. Phys. Chem. C* **2025**, *129*, 9646−9655.
(20) Lu, H.; Long, R. The Dynamic Rashba Effect Does Not Account for the Prolonged Charge Carrier Lifetime in Metal Halide Perovskites. *Nano Lett.* **2025**, *25*, 11005−11011.
(21) Hohenberg, P.; Kohn, W. Inhomogeneous Electron Gas. *Phys. Rev.* **1964**, *136*, B864−B871.
(22) Kohn, W.; Sham, L. J. Self-Consistent Equations Including Exchange and Correlation Effects. *Phys. Rev.* **1965**, *140*, A1133−A1138.
(23) Perdew, J. P.; Burke, K.; Ernzerhof, M. Generalized Gradient Approximation Made Simple. *Phys. Rev. Lett.* **1996**, *77*, 3865−3868.
(24) Grimme, S.; Ehrlich, S.; Goerigk, L. Effect of the Damping Function in Dispersion-Corrected Density Functional Theory. *J. Comput. Chem.* **2011**, *32*, 1456−1465.
(25) Rêgo, C. R. C.; Oliveira, L. N.; Tereshchuk, P.; Da Silva, J. L. F. Comparative Study of van der Waals Corrections to the Bulk Properties of Graphite. *J. Phys.: Condens. Matter* **2015**, *27*, 415502.
(26) Kresse, G.; Hafner, J. *Ab* Initio Molecular Dynamics for Open-Shell Transition Metals. *Phys. Rev. B* **1993**, *48*, 13115−13118.
(27) Blöchl, P. E. Projector Augmented-Wave Method. *Phys. Rev. B* **1994**, *50*, 17953−17979.
(28) Kresse, G.; Furthmüller, J. Efficient Iterative Schemes for *Ab* Initio Total-Energy Calculations Using a Plane-Wave Basis Set. *Phys. Rev. B* **1996**, *54*, 11169−11186.
(29) Ferreira, L. G.; Marques, M.; Teles, L. K. Slater Half-Occupation Technique Revisited: The LDA-1/2 and GGA-1/2 Approaches for Atomic Ionization Energies and Band Gaps in Semiconductors. *AIP Adv.* **2011**, *1*, 032119.
(30) Guedes-Sobrinho, D.; Caldeira, C. R.; Da Silva, G. R.; Da Silva, H. R.; Wenzel, W.; Piotrowski, M. J.; Cavalheiro Dias, A. Theoretical Exploration of Structural and Excitonic Properties in Black Phosphorus: From First-Principles to a Semi-Empirical Approach. *J. Phys. Chem. C* **2024**, *128*, 7242−7251.
(31) Mostofi, A. A.; Yates, J. R.; Lee, Y.-S.; Souza, I.; Vanderbilt, D.; Marzari, N. Wannier90: A Tool for Obtaining Maximally-Localised Wannier Functions. *Comput. Phys. Commun.* **2008**, *178*, 685−699.
(32) Salpeter, E. E.; Bethe, H. A. A Relativistic Equation for Bound-State Problems. *Phys. Rev.* **1951**, *84*, 1232.
(33) Dias, A. C.; Silveira, J. F.; Qu, F. WanTiBEXOS: A Wannier-Based Tight Binding Code for Electronic Band Structure, Excitonic and Optoelectronic Properties of Solids. *Comput. Phys. Commun.* **2023**, *285*, 108636.
(34) Reho, R.; Botello-Méndez, A. R.; Sangalli, D.; Verstraete, M. J.; Zanolli, Z. Excitonic response in transition metal dichalcogenide heterostructures from first principles: Impact of stacking, twisting, and interlayer distance. *Phys. Rev. B* **2024**, *110*, 035118.
(35) Bonadio, A.; Sabino, F. P.; Freitas, A. L.; Felez, M. R.; Dalpian, G. M.; Souza, J. A. Comparing the cubic and tetragonal phases of mapbi3 at room temperature. *Inorg. Chem.* **2023**, *62*, 7533−7544.
(36) Biega, R.-I.; Bokdam, M.; Herrmann, K.; Mohanraj, J.; Skrybeck, D.; Thelakkat, M.; Retsch, M.; Leppert, L. Dynamic Distortions of Quasi-2D Ruddlesden−Popper Perovskites at Elevated Temperatures: Influence on Thermal and Electronic Properties. *JPhysChemC* **2023**, *127*, 9183−9195.
(37) Li, Y.; Zhou, H.; Xia, M.; Shen, H.; Wang, T.; Gao, H.; Sheng, X.; Han, Y.; Chen, Z.; Dou, L. others Phase-pure 2D tin halide perovskite thin flakes for stable lasing. *Sci. Adv.* **2023**, *9*, No. eadh0517.
(38) Dalmedico, J.; Silveira, D.; O. de Araujo, L.; Wenzel, W.; Rêgo, C.; Dias, A.; Guedes-Sobrinho, D.; Piotrowski, M. J. Tuning Electronic and Structural Properties of Lead-Free Metal Halide Perovskites: A Comparative Study of 2D Ruddlesden-Popper and 3D Compositions. *ChemPhysChem* **2024**, *25*, No. e202481603.
(39) Semenova, O.; Yudanova, E.; Yeryukov, N.; Zhivodkov, Y.; Shamirzaev, T.; Maximovskiy, E.; Gromilov, S.; Troitskaia, I. Perovskite $CH_3NH_3PbI_3$ crystals and films. Synthesis and characterization. *J. Cryst. Growth* **2017**, *462*, 45−49.
(40) Jiang, L.; Wu, T.; Sun, L.; Li, Y.-J.; Li, A.; Lu, R.; Zou, K.; Deng, W.-Q. First-Principles Screening of Lead-Free Methylammonium Metal Iodine Perovskites for Photovoltaic Application. *J. Phys. Chem. C* **2017**, *121*, 24359−24364.
(41) Huang, Y.; Su, J.; Li, Q.; Wang, D.; Xu, L.; Bai, Y. Structure, optical and electrical properties of $CH_3NH_3SnI_3$ single crystal. *Physica B Condens. Matter* **2019**, *563*, 107−112.
(42) Gélvez-Rueda, M. C.; Peeters, S.; Wang, P.-C.; Felter, K. M.; Grozema, F. C. Effect of structural defects and impurities on the excited state dynamics of 2D BA_2PbI_4 perovskite. *Helv. Chim. Acta* **2020**, *103*, No. e2000121.
(43) Hansen, K. R.; McClure, C. E.; Powell, D.; Hsieh, H.-C.; Flannery, L.; Garden, K.; Miller, E. J.; King, D. J.; Sainio, S.; Nordlund, D. others Low exciton binding energies and localized exciton−polaron states in 2D tin halide perovskites. *Adv. Opt. Mater.* **2022**, *10*, 2102698.
(44) Glazer, A. M. The Classification of Tilted Octahedra in Perovskites. *Acta Crystallogr., Sect. B: Struct. Crystallogr. Cryst. Chem.* **1972**, *28*, 3384−3392.
(45) Sukmas, W.; Pinsook, U.; Tsuppayakorn-aek, P.; Pakornchote, T.; Sukserm, A.; Bovornratanaraks, T. Organic Molecule Orientations and Rashba−Dresselhaus Effect in α−Formamidinium Lead Iodide. *J. Phys. Chem. C* **2019**, *123*, 16508−16515.